

Organoselenium mild electrophiles in the inhibition of M^{pro} and SARSCoV-2 replication

Luca Sancineto,¹ Francesca Mangiavacchi,¹ Agnieszka Dabrowska^{2,3}, Agata Pacuła,⁴ Magdalena Obieziurska-Fabisiak,⁴ Cecilia Scimmi,¹ Ying Lei,⁵ Juan Kong,⁵ Yao Zhao,⁵ Karina dos Santos Machado,⁶ Adriano Velasque Werhli,⁶ Gianluca Ciancaleoni,⁷ Vanessa Nascimento⁸ Anna Kula-Pacurar², Eder Joao Lenardao,⁹ Haitao Yang,⁵ Jacek Ścianowski,⁴ Krzysztof Pyrc², and Claudio Santi^{1*}.

- 1 Department of Pharmaceutical Sciences, University of Perugia, Via del Liceo, 1 06100 Perugia (PG), Italy
- 2 Virogenetics Laboratory of Virology, Malopolska Centre of Biotechnology, Jagiellonian University, Gronostajowa 7a, 30–387 Krakow, Poland.
- 3 Microbiology Department, Faculty of Biochemistry, Biophysics and Biotechnology, Jagiellonian University, Gronostajowa 7, 30-387 Krakow, Poland.
- 4 Department of Organic Chemistry, Faculty of Chemistry, Nicolaus Copernicus University, 7 Gagarin Street, Torun, Poland
- 5 Shanghai Institute for Advanced Immunochemical Studies and School of Life Science and Technology, ShanghaiTech University, Shanghai, China
- 6 Laboratório de Biologia Computacional, Centro de Ciências Computacionais, Universidade Federal do Rio Grande - FURG, Avenia Itália, km 8, 96201-900, Rio Grande, RS, Brazil
- 7 Dipartimento di Chimica e Chimica Industriale (DCCI) Università di Pisa Via Giuseppe Moruzzi, 13 - 56124 Pisa, Italy
- 8 Departamento de Química Orgânica, Universidade Federal Fluminense, Laboratório de Síntese e Aplicação de Substâncias Supramoleculares e Organocalcogenios (SupraSelen), Outeiro Sao Joao Batista s/n, 24020-141, Niteroi, RJ, Brazil
- 9 Laboratory of Clean Organic Synthesis, Federal University of Pelotas, Pelotas, RS, Brazil

Introduction

After the severe acute respiratory syndrome (SARS) and the middle-east respiratory syndrome (MERS) caused by coronaviruses in 2003 [1] and 2012 [2], respectively, the unprecedentedly rapid emergence of a severe acute respiratory syndrome associated with the new coronavirus (Sars-CoV-2) and the resulting disease COVID-19 strongly polarized research efforts in an attempt to develop vaccines, therapeutic procedures and small molecules having a selective antiviral activity. Unfortunately, despite the identification of several molecular targets [3–5], the number of molecules necessary to drive a concrete drug discovery program is still very limited, and most of the current studies focus on repurposed drugs [6].

In a recent high-throughput screening study, the attractive organoselenium compound 2-phenyl-1,2-benzoselenazol-3-one (Ebselen, compound **1**) [7] has been identified as the most potent inhibitor of the main protease (M^{pro}), among a pool of existing small-molecule drugs [8]. Subsequently, it was also demonstrated that it potentially inhibits SARS-CoV-1 and SARS-CoV-2 papain-like proteases (PL^{pro}) [9].

M^{pro} and PL^{pro} are two viral-encoded enzymes important for viral replication and to escape the host immune response. The lack of closely related cellular homologs makes them attractive targets for the development of coronavirus-directed antivirals.

When tested *in vitro*, Ebselen (compound **1**, Figure 1) showed a potent inhibitory activity toward M^{pro} with an IC₅₀ in the nanomolar range (670 nM). Furthermore, it showcased a micromolar antiviral activity measured in a cellular context (IC₅₀ = 4.67 μM). These data make Ebselen the most potent M^{pro} and SARS-CoV-2 replication inhibitor known to date [9]. The second protease encoded in the coronaviral genome, PL^{pro}, is also efficiently inhibited by such organoselenium compound, even if with lower potency (IC₅₀ = 2.26 μM) [8].

Mode of action studies revealed that both enzymes are irreversibly inhibited by compound **1** that is able to covalently bind to reactive cysteines within the PL^{pro} and M^{pro} active sites, forming a stable selenyl sulfide. Tandem mass spectrometry and computational calculations proved that the reactive

cysteine in M^{pro} is Cys145 [4,10], while molecular modeling efforts demonstrated that Cys111 is the target of Ebselen within the PL^{pro} active site [8].

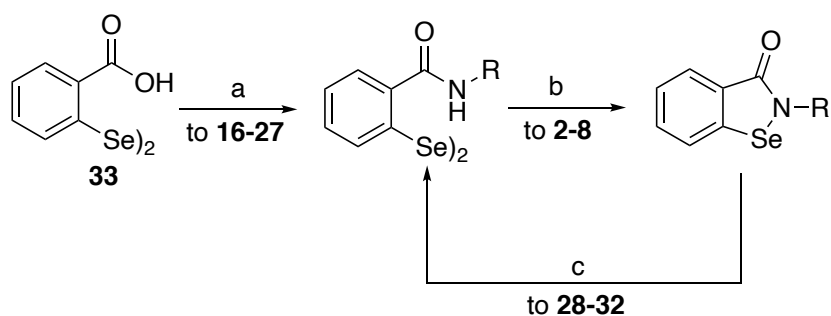
The capability of Ebselen to randomly modify cysteines is already known [11–15], and for someone, it could represent a critical issue on its actual clinical exploitability, even if several different examples demonstrate the almost complete absence of toxic effects *in vivo*, proved also by the many clinical trials in which it was and it is still involved [16]. Furthermore, it showed several positive effects exploitable in the context of COVID-19 [17].

Taken together, these results clearly underline the value of Ebselen as a lead compound and, at the same time, raise the intriguing question on whether its chemical reactivity could be exploited and directed to selectively target specific cysteines on the active sites of selected enzymes by modifications in its structure.

We recently reported a novel and efficient method to prepare variously decorated Ebselen-like derivatives starting from *ortho*-(amido)aryldiselenides [17], including the DiSeBAs, a class of compounds that potently reduce HIV replication [18], by inhibiting the key viral protein NCp7 [19,20]. In our ongoing work in the field of organoselenium chemistry, and in an attempt to understand the molecular mechanism behind the biological properties of organoselenium compounds, we herein compare the anti SARS-CoV-2 M^{pro} activity of a series of diselenides (compounds **16-34**) and Ebselen-like derivatives (compounds **2-15**). Such a comparison has been scarcely explored yet, and could be beneficial to enlarge the classes of small molecules able to inhibit M^{pro} [21].

Results and Discussion

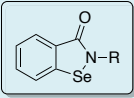
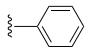
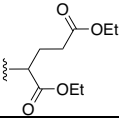
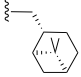
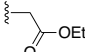
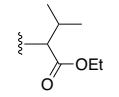
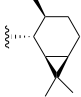
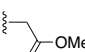
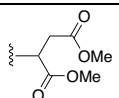
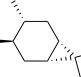
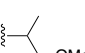
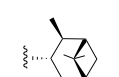
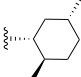
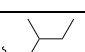
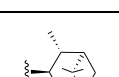
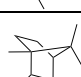
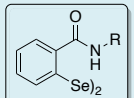
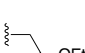
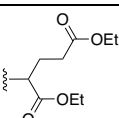
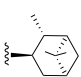
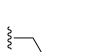
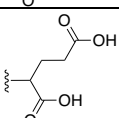
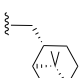
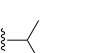
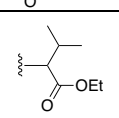
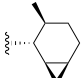
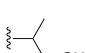
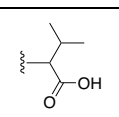
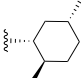
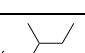
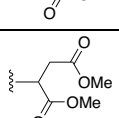
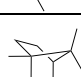
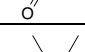
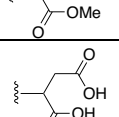
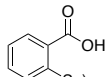
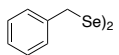
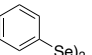
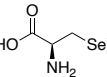
Diphenyl diselenide (compound **36**) and selenocystine (compound **34**) are commercially available. All the other compounds were synthesized. Dibenzyl diselenides (compound **35**) was prepared following the reported procedure [21]. Ebselen-like compounds **2-8** were prepared starting from **33** [21,22], which was first coupled with amino acids protected as esters leading to compound **16-27** [18] (Scheme 1, step a). The ester derivatives were converted into the corresponding benzoselenazolone following a recently reported procedure (Scheme 1, step b) [23]. Diselenides (**28-32**) were prepared from the corresponding Ebselen-like compounds (**10-12, 14 and 15**) via a sequential NaBH₄-mediated reduction of the Se-N bond and air oxidation of the so formed selenolate anion. (Scheme 1, step c) [24,25].



Scheme 1. Synthesis of diselenides and benzoselenazolones.

As first line of screening, they were all preliminary assayed at the concentration of 40 μ M, showing full inhibition of the enzymatic activity. Then, the half maximal inhibitory concentration (IC₅₀) was determined and the results are collected in Table 1.

Table 1. Structures and IC₅₀s of all the tested the compounds.

								
entry	R	IC ₅₀ ,nM	entry	R	IC ₅₀ ,nM	entry	R	IC ₅₀ ,nM
1 Ebselen		121 ± 46.5 670 [9]	6		101.5 ± 39.5	11		518.9 ^a
2		201.4 ± 24.3	7		56.30 ± 31.1	12		311.5 ^a
3		166.8 ± 41.0	8		101.16 ± 97.4	13		487.2 ^a
4		149.5 ± 18.1	9		358.8 ^a	14		346.2 ^a
5		87.64 ± 19.8	10		334.9 ^a	15		203.2 ^a
a) acquired as a single experiment								
								
entry	R	IC ₅₀ ,μM	entry	R	IC ₅₀ ,μM	entry	R	IC ₅₀ ,μM
16		0.56 ± 0.21	22		6.28 ± 4.04	28		ND
17		6.49 ± 1.36	23		> 100	29		6.133 ^a
18		1.06 ± 0.23	24		1.39 ± 0.09	30		3.449 ^a
19		5.44 ± 1.86	25		4.87 ± 2.97	31		8.332 ^a
20		1.26 ± 0.36	26		1.92 ± 0.68	32		43.16 ^a
21		5.14 ± 2.39	27		11.84 ± 2.48			
a) acquired as a single experiment								
entry	cmpd	IC ₅₀ ,μM	entry	cmpd	IC ₅₀ ,μM	entry	cmpd	IC ₅₀ ,μM
33		> 100	35		ND	36		1.87 ± 0.26
34		64.86 ^a						

a) acquired as a single experiment

The Ebselen derivatives (**2-15**) resulted in all the cases more potent than their corresponding diselenides analogues **16-36**, confirming that the electrophilic character of the selenium atom is the key characteristic for the reaction with the sulfur atom of the cysteine. In the Ebselen derivatives, the nitrogen-selenium bond reduces the electronic density of the chalcogen, whereas in the diselenides, the non-bonding interaction between the amidic oxygen and the selenium atom only slightly contribute on improving the electrophilic character of Se. This can be also partially evidenced by the ^{77}Se -NMR chemical shift that ranges from 804 to 935 ppm for benziisoselenazolones, and from 439 to 450 ppm for the corresponding diselenides.

In addition, the geometry of some selected Ebselen-like and diselenides systems has been optimized by DFT (b3lyp-d3/def2-tzvp level of theory) and the natural partial atomic charges have been computed by using the Natural Population Analysis (NPA) as implemented in the NBO software suite. The results are shown in Table 2

Table 2. NPA partial charge (in e) on the selenium atom (two values are shown for diselenide systems) on some ebselen-like and diselenides systems.			
compound	q(Se)	compound	q(Se)
1	0.607	24	0.165/0.167
3	0.613	30	0.143/0.175
5	0.619	33	0.173/0.186
7	0.617	34	0.104/0.122
12	0.608	36	0.151/0.153

There is a qualitative inverse proportionality between $q(\text{Se})$ and IC_{50} : compounds having $q(\text{Se}) > 0.610$ e are the most active ones, whereas below this threshold we found less active systems as **1** and **12**. For the least active compounds, $q(\text{Se})$ is less than 0.2 e. This suggests the hypothesis of a nucleophilic attack of the sulfur of the cysteine to the selenium. The exact reaction mechanism is under study.

The benziisoselenazolone derivatives displayed values of IC_{50} s in the nanomolar range, with the ones bearing a carboxylic moiety showing slightly better results (compounds **2-8**). Among these, valine and isoleucine derivatives (compounds **7** and **5** respectively) showcased the best results. Terpene-based benziisoselenazolones (compounds **9-15**) are weaker if compared to the ester containing ones, but still very potent, better than Ebselen. These results seem indicate that a hydrogen bond acceptor group, one carbon far from the benziisoselenazolone scaffold, is beneficial for the enzymatic inhibition.

With the only exception of selenocystine (compound **34**), which showed an IC_{50} of 64 μM and compounds **23**, **28**, **32**, **33** and **35**, which were unable to inhibit M^{pro} even at a concentration superior of 100 μM , all of the diselenides derivatives inhibited the protease activity at low micromolar concentrations or at submicromolar levels, as observed for the glycine derivative (compound **16**). Diphenyl diselenides, the simplest among the aromatic diselenides that we have tested, showed activity with IC_{50} of 1.87 μM . Structure-activity relationship information for this class of compounds clearly highlighted that the presence of the ester moiety is better than the free carboxylic acids (compound **16** vs **17**, **18** vs **19**, and so on). Hydrocarbon-containing diselenides (**29-31**) are endowed with anti- M^{pro} activity superimposable to that of the diselenides with a free carboxylic acid group. Tables 3 and 4 present the docking simulations results as well as M^{pro} -compounds interactions. According to these Vina docking results, all the compounds presented favorable estimated free energy of binding (FEB). Ebselen and Ebselen derivatives (**1-15**) have an average FEB of -6.56 ± 0.46 kcal/mol for both babel molecules and -6.22 ± 0.61 kcal/mol for MOPAC. The correspondent diselenides analogues **16-36** have -7.31 ± 1 kcal/mol for babel conjugate gradient, -7.05 ± 0.83 kcal/mol for babel steepest descent and -6.84 ± 0.81 kcal/mol for MOPAC. Thus, according to these

results, all the compounds are good inhibitor candidates for M^{pro} with a small difference in average FEB for diselenides probably because they have more atoms and these number are taken into consideration in Vina score.

Table 3. Docking results and non-bonded M ^{pro} -benzisoselenazolones interactions										
cmpd	Vina FEB (<i>kcal/mol</i>)			Amino acids in non-bonded contacts MOPAC best docking results (LigPlot+ analysis)						
	Babel Conjugate Gradient	Babel Steepest Descent	MOPAC PM6	CYS 145	GLY 143	ASN 142	HIS 41	GLU 166	MET 165	GLN 189
1	-6.6	-6.1	-6.6	Y	Y	Y	Y	Y		Y
2	-6.3	-5.5	-5.9	Y	Y			Y		
3	-6.0	-5.3	-6.2	Y	Y			Y		
4	-6.1	-5.6	-6.1	Y	Y			Y		
5	-6.0	-5.6	-6.3	Y	Y		Y	Y		Y
6	-7.0	-6.2	-6.2	Y		Y		Y		Y
7	-6.4	-5.3	-5.7	Y		Y	Y	Y	Y	Y
8	-6.0	-6.2	-6.5	Y	Y		Y	Y		
9	-6.9	-6.7	-6.7	Y	Y		Y	Y		Y
10	-6.7	-7.1	-6.6	Y		Y		Y		
11	-7.0	-7.0	-6.9	Y		Y	Y	Y	Y	Y
12	-6.9	-6.7	-6.2	Y				Y		Y
13	-7.3	-7.0	-6.7	Y	Y	Y		Y		
14	-6.1	-6.0	-6.2	Y	Y	Y	Y			Y
15	-7.1	-6.8	-6.3	Y	Y		Y	Y		Y
Av	-6.56	-6.56	-6.22							
SD	0.46	0.46	0.62							

Docking simulations performed with Vina: columns 3, 4 and 5 present the estimated free energy of binding FEB in kcal/mol according to the molecules optimized with three different methodologies. The following columns describe if there is (Y) or not a non-bonded interaction (according to LigPlot+) between M^{pro} key amino acids and the MOPAC optimized molecules according to the best ranked docking result.

Table 4. Docking results and non-bonded M^{pr}-diselenides interactions

cmpd	Vina FEB (kcal/mol)			Amino acids in non-bonded contacts MOPAC best docking results						
	Babel Conjugate Gradient	Babel Steepest Descent	MOPAC PM6	CYS 145	GLY 143	ASN 142	HIS 41	GLU 166	MET 165	GLN 189
16	-7.2	-6.8	-7.5	Y	Y		Y			Y
17	-8.3	-7.8	-8.3		Y					Y
18	-7.1	-7.0	-7.6				Y		Y	Y
19	-7.8	-7.5	-8.4				Y		Y	
20	-7.1	-5.9	-7.4	Y			Y		Y	Y
21	-7.7	-6.9	-7.8				Y		Y	Y
22	-6.2	-6.5	-6.8		Y		Y		Y	Y
23	-7.4	-7.0	-7.4				Y		Y	Y
24	-6.9	-6.3	-6.8	Y		Y	Y		Y	
25	-6.5	-6.9	-8.0				Y		Y	Y
26	-7.2	-6.4	-7.5				Y		Y	Y
27	-7.0	-6.6	-8.3				Y		Y	
28	-7.7	-7.2	-8.1	Y		Y				Y
29	-8.1	-6.8	-7.9	Y	Y					Y
30	-8.3	-7.0	-7.8	Y			Y			
31	-7.1	-5.9	-6.4							Y
32	-6.9	-6.6	-7.5		Y	Y				
33	-7.0	-6.3	-7.0	Y			Y			
34	-5.3	-4.9	-5.8				Y			Y
35	-5.7	-5.7	-5.9				Y		Y	
36	-5.6	-5.3	-6.1	Y	Y					Y
Av	-7.31	-7.05	-6.84							
SD	1	0.83	0.81							

Docking simulations performed with Vina: columns 3, 4 and 5 present the estimated free energy of binding FEB in kcal/mol according to the molecules optimized with three different methodologies. The following columns describe if there is (Y) or not a non-bonded interaction (according to LigPlot+) between Mpro key amino acids and the MOPAC optimized molecules according to the best ranked docking result.

Regarding the docking results, about the interactions between M^{pro} amino acids and the compounds (Table 4) it is possible to see that compounds **1-15** had better docking scores preferably close to the P1', P2 and P3 M^{pro} sites [9] presenting non-bonded contacts with CYS 145, HIS 41 and GLU 166. Figure 1 shows in detail compounds **5** and **7** non-bounded and hydrophobic contacts with M^{pro} generated by Discovery Studio 2020 (BIOVIA 2020). As we can see, compound **5** established hydrophobic contacts and pi-sulfur bonds with CYS 145 (P1' site) close to the selenium atom, hydrogen bonds with GLY 143 (P1' site) and Pi hydrophobic bonds with HIS 41 (P2 site). benzisoselenazolone **7** also shows hydrophobic contacts with CYS 145 and Pi hydrophobic bonds with HIS 41 (P2 site).

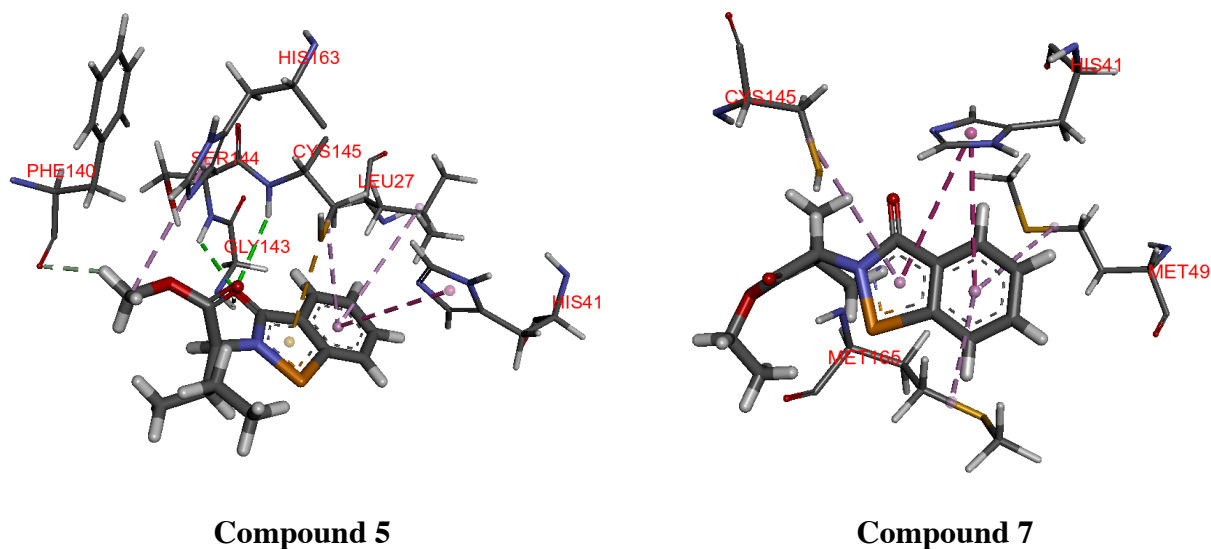


Figure 1. M^{pro} -compounds interactions of the MOPAC best docking result for compounds **5** and **7**. Analyses performed by Discovery Studio 2020 (BIOVIA 2020). Green dashed lines correspond to classical hydrogen bonds. Soft Green dashed lines correspond to non-classical hydrogen bonds (Carbon Hydrogen bond and Pi donor Hydrogen bond). Hydrophobic contacts are in pink and magenta dashed lines (Pi/Alkyl Hydrophobic). Sulfur contacts in Orange. Carbon atoms are in dark gray, hydrogen atoms in light gray, Oxygen in red, Selenium in Orange and Nitrogen in blue, Sulfur in yellow.

Regarding MOPAC docking results (Table 2, columns 4-10) the non-bonded contacts are not very frequent between compounds **16-36** compared to compounds **1-15**. In addition, GLU 166 does not present any non-bonded contact with these molecules and contact with GLN 189 is more frequent. In order to exemplify these differences, we show in Figure 2 the compounds **19** and **36** non-bounded and hydrophobic contacts with M^{pro} obtained by Discovery Studio 2020 (BIOVIA 2020). For both molecules GLN 189 (P4 site) is interacting.

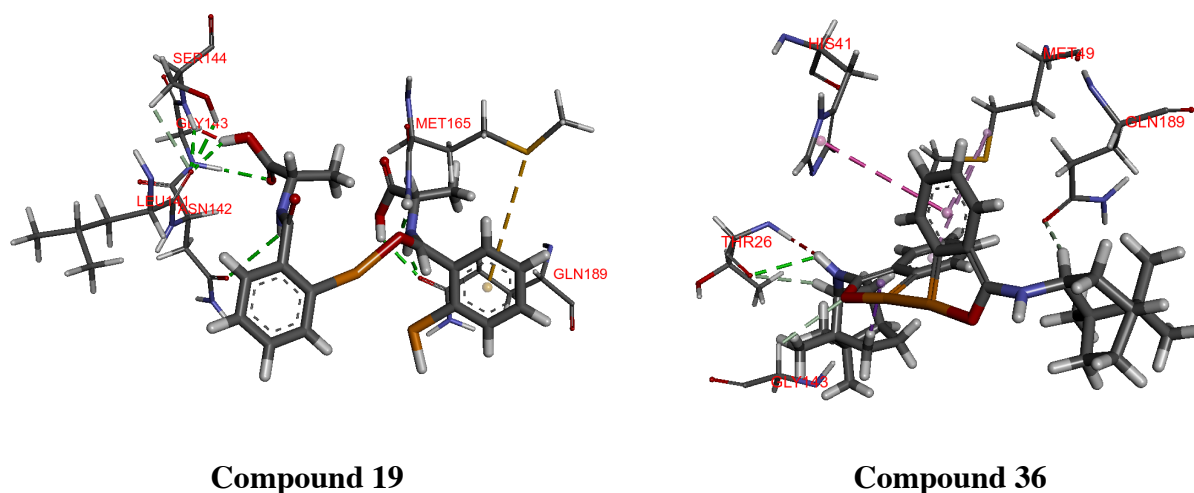
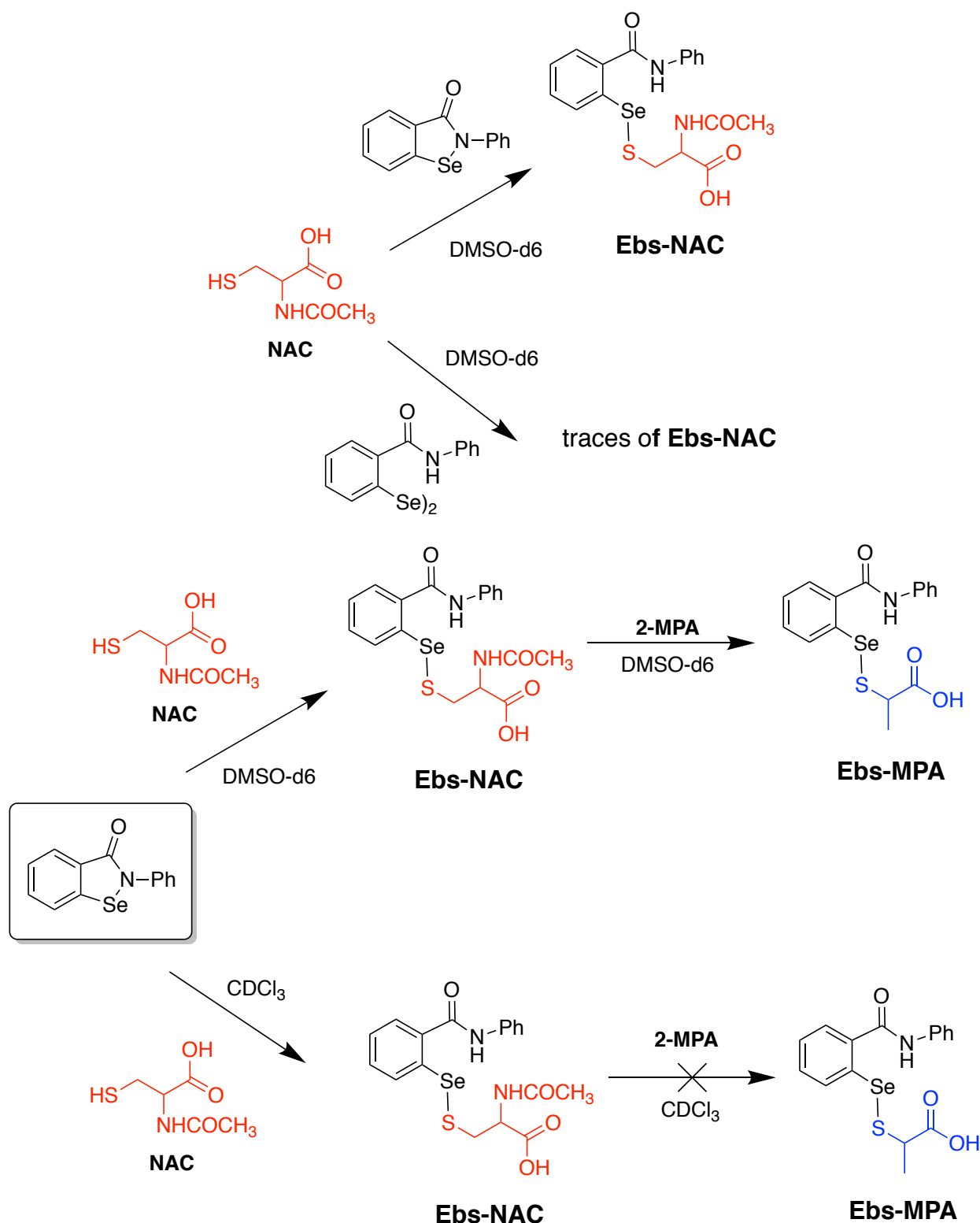


Figure 2. Mpro-compounds interactions of the MOPAC best docking result for compounds **19** and **36**. Analyses performed by Discovery Studio 2020 (BIOVIA 2020). Green dashed lines correspond to classical hydrogen bonds. Soft Green dashed lines correspond to non-classical hydrogen bonds (Carbon Hydrogen bond and Pi donor Hydrogen bond). Hydrophobic contacts are in rose and magenta dashed lines (Pi/Alkyl Hydrophobic). Sulfur contacts in Orange. Carbon atoms are in dark gray, Hydrogen atoms in light gray, Oxygen in red, Selenium in Orange and Nitrogen in blue.

As we can see on Figures 1,2 and Table 2, the non-bonded and hydrophobic contacts with CYS 145 (close to the selenium atoms) is more frequent on MOPAC docking results with molecules **1-15**. Thus, even docking FEB scores do not show difference between ebselen derivatives and diselenides derivatives, the non-bonded and hydrophobic contacts can help to explain that molecules **1-15** presented better activity maybe because their interactions with CYS 145 and preferences by the P1' and P3 M^{pro} sites while diselenides derivatives molecules presented preferences to be close to P4 site. In order to simulate the chemical reaction between a free cysteine with the selenium electrophiles and the corresponding thiol exchange that could account for a detoxification process mediated in cells by glutathione, some ⁷⁷Se-NMR experiments were setup. Ebselen (0.125M; 13.7 mg, 0.05 mmol in 0.4 mL) and the corresponding diselenide (0.125M; 27.6 mg, 0.05 mmol in 0.4 mL) were solubilized in DMSO-d₆ and separately reacted with a stoichiometric amount of N-acetyl cysteine (NAC). Ebselen was rapidly and quantitatively transformed into the corresponding Se-S (Ebs-NAC) adduct, evidenced by the appearance of the peak at 551.2 ppm and the complete disappearance of the peak at 912.4 ppm. On the contrary, in the case of diselenides, the same reaction conditions afforded only traces of the Ebs-NAC adduct, reflecting the different electrophilic reactivity of the selenium atom in the two different molecules. The formed Ebs-NAC adduct was treated with 1 equivalent of 2 mercaptopropionic acid observing the slow formation of a second adduct (Ebs-MPA with a peak in the ⁷⁷Se-NMR at 525.8 ppm) arising from a thiol exchange. When the same reaction was repeated in CDCl₃, the thiol exchange was not observed neither after the addition of a large excess of 2 mercaptopropionic acid, and indicating that this reaction follows a S_N2 mechanisms.



Scheme 2. NMR experiments of thiol exchange on ebselen and its corresponding diselenides.

We then moved to analyze whether the anti M^m activity translates into the inhibition of the SARS-CoV-2 replication in a cellular context. To this aim, benzisoselenazolones **2**, **3**, **5-8**, and diselenides **16**, **17**, **20**, **24**, and **25** were selected. The ability to inhibit SARS-CoV-2 replication by the compounds was determined by infecting confluent monolayers of Vero cells in the presence of a chosen compound. The compounds were present on cells during and after the inoculation process. After 2

days of culturing at 37°C, the toxicity of the compound and the virus-associated cytopathic effect (CPE) reduction was scored. The results are presented in Table 5.

Compound	Concentration μM		
	50	10	5
1	Tox	+	-
2	Tox	+	-
3	Tox	+/-	-
5	-	-	-
6	Tox	-	-
7	+	-	-
8	Tox	-	-
16	Tox	+/-	-
17	-	-	-
20	-	-	-
24	+	-	-
25	+/-	-	-

(+) CPE reduction; (-) no CPE reduction; (+/-) inconclusive observations: CPE reduction in one experiment, no CPE reduction in the other experiment; (tox) cytotoxicity observed.

When CPE reduction was evident (**1-3, 7, 16, 24, 25**), cell culture supernatants were collected and total viral RNA was isolated, reversely transcribed, and used as a template for real-time quantitative PCR (qPCR) reaction. The number of viral RNA copies per milliliter was estimated based on the serial dilutions of DNA standards. The experiment was performed in two biological replications, each sample at least in a triplicate. Obtained data were normalized, tested with Shapiro-Wilk normality test, and Kruskal-Wallis with Dunn's multiple comparison test. The results are presented in **Figure 3**.

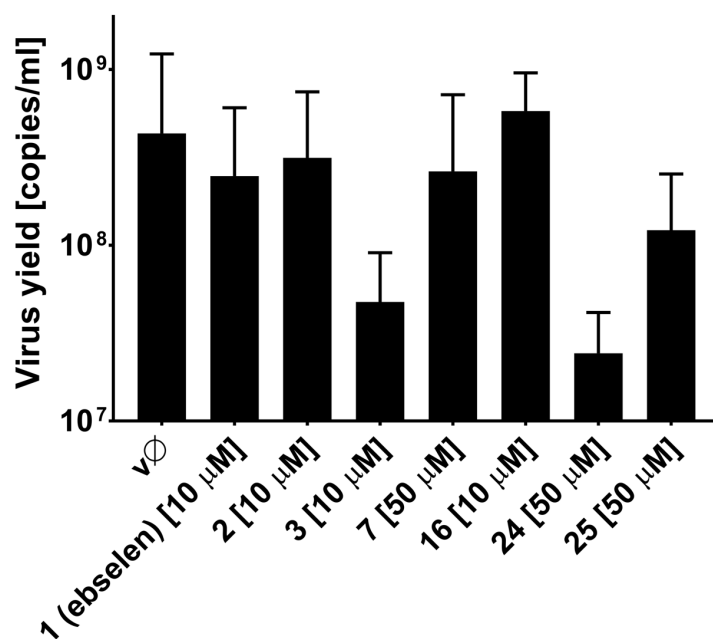


Figure 3. Inhibition of SARS-CoV-2 infection in Vero cells by selected compounds.

The most potent compounds are the benzenoselenazolone derivative **3** and the diselenide **24**, when the virus was inhibited by 10 times. Compounds **2**, **25**, **7**, and Ebselen (**1**) only slightly reduce SARS-CoV-2 infection (<0.5 log), whereas compound **16** does not affect SARS-CoV-2 replication.

Conclusion:

Based on the here reported data, all the Ebselen-like derivatives resulted to be very strong in vitro inhibitors of SARS-CoV-2 main protease. We demonstrated that this activity mainly depends on the electrophilicity of the selenium atom that is considerably higher in the N-substituted 1,2-benzoselenazol-3(2H)-ones respect to the corresponding diselenides allowing it to be rapidly attached by free thiols affording sulfur-selenium intermediates that are further subjected to thiol exchange processes. This data paints a very complex scenario that requires us to consider Ebselen and Ebselen-like derivatives as potential electrophilic substrates for the several other free thiols present in the cell beside the target free cysteine. The sulfur selenium intermediates are milder electrophiles that could be theoretically implicated in both the detoxification process as well as in the final enzymatic inhibition. We here demonstrated that the in vitro inhibition activity is not fully reproduced in the prevention of viral replication in the cell-based assay. This indicate that the structure of the substituents introduced in the Ebselen scaffold is a crucial factor to control the reactivity of the selenated molecule in the network of thiol exchanges, as well as for molecular recognition of the targeted enzymatic cysteine. For this reason, an in-depth investigation is strongly desirable to better understand how to increase the activity and the selectivity of Ebselen derivatives overcoming the issues of the apparent PAINS-like role of Ebselen.

Furthermore, besides the antiviral activity, thee selected compounds also showed a different ability to reduce the virus-induced cytopathic effect, indicating that other mechanisms could be implicated. One may consider here the well-known cytoprotective antioxidant activity of Ebselen and its derivatives.

Experimental:

Synthesis of diselenides 28-32

To a solution of benzenoselenazolone **10-12**, and **14-15** (1.0 mmol) in methanol (10 mL) cooled to 0°C, sodium borohydride (1.0mmol) was added and the mixture was stirred for 1h. Water (15mL) was added and the mixture was oxidized with air for 1h. The formed precipitate was filtered and dried in air. Yields **28** – 72%, **29** – 63%, **30** – 69%, **31** – 70%, **32** – 81%.

Molecular Docking Simulations

In order to perform protein-ligand molecular docking simulations it is necessary the 3D structures of the target protein and the proposed compounds. Different structures of main protease (M^{pro}) are deposited on Protein Data Bank from which we chose to consider 6LU7 [4]. We have chosen this structure since it was one of the first structures of Mpro of SARS-CoV-2, it has a resolution of 2.16 Å, no missing amino acids and it was crystallographed with N3 compound on the binding site. All the proposed compounds were prepared from the SMILES using three different algorithms for 3D geometry optimization: software babel with conjugate gradient and steepest descent algorithms [26] and MOPAC with PM6 [27].

All docking simulations were performed using Vina [28] with python scripts generated by FrameworkVS [29]. The grid box was defined with size of x , y and $z = 22 \text{ \AA}$ and *center of* $x = -9.342 \text{ \AA}$; *center of* $y = 10.088 \text{ \AA}$; *center of* $z = -22.476 \text{ \AA}$. We evaluated protein-ligand interactions using LigPlot+ [30] and Discovery Studio [BIOVIA, 2020].

Since MOPAC optimization determines charges for Selenium atoms we investigated the compounds interactions with some M^{pro} key amino acids in N3 sites [4] P1' (CYS 145 and GLY 143), P1 (ASN 142), P2 (HIS 41), P3 (MET 165, GLU 166) and P5 (GLN 189) .

Computational Details

All the geometries were optimized with ORCA 4.1.0, (Neese, F. *Software Update: The ORCA Program System, Version 4.0. Wiley Interdiscip. Rev. Comput. Mol. Sci. 2017, 8 (1), e1327. <https://doi.org/10.1002/wcms.1327>*.) using the B3LYP functional and the RIJCOSX approximation in conjunction with a triple- ζ quality basis set (def2-tzvp). All the structures were confirmed to be local energy minima (no imaginary frequencies). Dispersion effects were accounted using the Grimme D3-parametrized correction with Becke – Johnson damping to the DFT energy. (S.Grimme, S.Ehrlich, L.Goerigk, *J Comput Chem*, (2011), 32, 1456-1465) Natural Population Analysis were performed using NBO 6. (NBO 6.0. E. D. Glendening, J. K. Badenhoop, A. E. Reed, J. E. Carpenter, J. A. Bohmann, C. M. Morales, C. R. Landis and F. Weinhold (*Theoretical Chemistry Institute, University of Wisconsin, Madison, WI, 2013*); <http://nbo6.chem.wisc.edu/>)

Cells and the virus

Vero E6 (*Cercopithecus aethiops*; kidney epithelial; CRL-1586) were cultured in Dulbecco's MEM (Thermo Fisher Scientific, Poland) supplemented with 3% fetal bovine serum (heat-inactivated; Thermo Fisher Scientific, Poland) and antibiotics: penicillin (100 U/ml), streptomycin (100 μ g/ml), and ciprofloxacin (5 μ g/ml). Cells were maintained at 37°C under 5% CO₂.

SARS-CoV-2 strain 026V-03883 was kindly granted by Christian Drosten, Charité – Universitätsmedizin Berlin, Germany by the European Virus Archive - Global (EVAg); <https://www.european-virus-archive.com/>).

All SARS-CoV-2 stocks were generated by infecting monolayers of Vero E6 cells. The virus-containing liquid was collected at day 3 post-infection (p.i.), aliquoted, and stored at –80°C. Control samples from mock-infected cells were prepared in the same manner. Virus yield was assessed by titration on fully confluent Vero E6 cells in 96-well plates, according to the method of Reed and Muench. Plates were incubated at 37°C for three days, and the cytopathic effect (CPE) was scored by observation under an inverted microscope.

Isolation of nucleic acids and reverse transcription

A viral DNA/RNA kit (A&A Biotechnology, Poland) was used for nucleic acid isolation from cell culture supernatants. RNA was isolated according to the manufacturer's instructions. cDNA samples were prepared with a high-capacity cDNA reverse transcription kit (Thermo Fisher Scientific, Poland), according to the manufacturer's instructions.

Quantitative PCR

Viral RNA was quantified using quantitative PCR (qPCR; CFX96 Touch real-time PCR detection system; Bio-Rad, Poland). cDNA was amplified using 1 \times qPCR master mix (A&A Biotechnology, Poland), in the presence of the probe (100 nM; FAM/BHQ1, ACT TCC TCA AGG AAC AAC ATT GCC A) and primers (450 nM each; CAC ATT GGC ACC CGC AAT C and GAG GAA CGA GAA GAG GCT TG). The heating scheme was as follows: 2 min at 50°C and 10 min at 92°C, followed by

30 cycles of 15 s at 92°C and 1 min at 60°C. In order to assess the copy number for the N gene, standards were prepared and serially diluted.

Acknowledgments:

The authors thanks University of Perugia for Fondo per la Ricerca di Base 2019. This work has been undertaken under the umbrella of the Selenium Sulfur Redox and Catalysis Network (SeSRedCat).

We are grateful to all members of Pyrc laboratories for helpful discussion. We would like to thank Katarzyna Owczarek, Artur Szczepanski and Pawel Botwina for their excellent technical support.

References:

1. Peiris, J.S.M.; Guan, Y.; Yuen, K.Y. Severe acute respiratory syndrome. *Nat. Med.* 2004.
2. Memish, Z.A.; Perlman, S.; Van Kerkhove, M.D.; Zumla, A. Middle East respiratory syndrome. *Lancet* **2020**, *395*, 1063–1077, doi:10.1016/S0140-6736(19)33221-0.
3. Cannalire, R.; Stefanelli, I.; Cerchia, C.; Beccari, A.R.; Pelliccia, S.; Summa, V. SARS-CoV-2 Entry Inhibitors: Small Molecules and Peptides Targeting Virus or Host Cells. *Int. J. Mol. Sci.* **2020**, *21*, 5707, doi:10.3390/ijms21165707.
4. Jin, Z.; Du, X.; Xu, Y.; Deng, Y.; Liu, M.; Zhao, Y.; Zhang, B.; Li, X.; Zhang, L.; Peng, C.; et al. Structure of Mpro from COVID-19 virus and discovery of its inhibitors. *bioRxiv* **2020**, 2020.02.26.964882, doi:10.1101/2020.02.26.964882.
5. Nadeem, M.S.; Zamzami, M.A.; Choudhry, H.; Murtaza, B.N.; Kazmi, I.; Ahmad, H.; Shakoori, A.R. Origin, Potential Therapeutic Targets and Treatment for Coronavirus Disease (COVID-19). *Pathogens* **2020**, *9*, 307, doi:10.3390/pathogens9040307.
6. Harrison, C. Drug researchers pursue new lines of attack against COVID-19. *Nat. Biotechnol.* **2020**, *38*, 659–662, doi:10.1038/d41587-020-00013-z.
7. Parnham, M.J.; Sies, H. The early research and development of ebselen. *Biochem. Pharmacol.* **2013**, *86*, 1248–1253, doi:10.1016/j.bcp.2013.08.028.
8. Węglarz-Tomczak, E.; Tomczak, J.; Talma, M.; Brul, S. Ebselen as a highly active inhibitor of PL Pro CoV2. *bioRxiv* **2020**, doi:10.1101/2020.05.17.100768.
9. Jin, Z.; Du, X.; Xu, Y.; Deng, Y.; Liu, M.; Zhao, Y.; Zhang, B.; Li, X.; Zhang, L.; Peng, C.; et al. Structure of Mpro from SARS-CoV-2 and discovery of its inhibitors. *Nature* **2020**, *582*, 289–293, doi:10.1038/s41586-020-2223-y.
10. Menéndez, C.A.; Byléhn, F.; Perez-Lemus, G.R.; Alvarado, W.; de Pablo, J.J. Molecular characterization of Ebselen binding activity to SARS-CoV-2 main protease. *Sci. Adv.* **2020**, eabd3045, doi:10.1126/sciadv.abd0345.
11. Mukherjee, S.; Weiner, W.S.; Schroeder, C.E.; Simpson, D.S.; Hanson, A.M.; Sweeney, N.L.; Marvin, R.K.; Ndjomou, J.; Kolli, R.; Isailovic, D.; et al. Ebselen Inhibits Hepatitis C Virus NS3 Helicase Binding to Nucleic Acid and Prevents Viral Replication. *ACS Chem. Biol.* **2014**,

9, 2393–2403, doi:10.1021/cb500512z.

12. Chiou, J.; Wan, S.; Chan, K.-F.; So, P.-K.; He, D.; Chan, E.W.; Chan, T.; Wong, K.; Tao, J.; Chen, S. Ebselen as a potent covalent inhibitor of New Delhi metallo- β -lactamase (NDM-1). *Chem. Commun.* **2015**, *51*, 9543–9546, doi:10.1039/C5CC02594J.
13. Favrot, L.; Grzegorzewicz, A.E.; Lajiness, D.H.; Marvin, R.K.; Boucau, J.; Isailovic, D.; Jackson, M.; Ronning, D.R. Mechanism of inhibition of Mycobacterium tuberculosis antigen 85 by ebselen. *Nat. Commun.* **2013**, *4*, 2748, doi:10.1038/ncomms3748.
14. Thenin-Houssier, S.; de Vera, I.M.S.; Pedro-Rosa, L.; Brady, A.; Richard, A.; Konnick, B.; Opp, S.; Buffone, C.; Fuhrmann, J.; Kota, S.; et al. Ebselen, a Small-Molecule Capsid Inhibitor of HIV-1 Replication. *Antimicrob. Agents Chemother.* **2016**, *60*, 2195–2208, doi:10.1128/AAC.02574-15.
15. Leroux, F.; Bosc, D.; Beghyn, T.; Hermant, P.; Warenghem, S.; Landry, V.; Pottiez, V.; Guillaume, V.; Charton, J.; Herledan, A.; et al. Identification of ebselen as a potent inhibitor of insulin degrading enzyme by a drug repurposing screening. *Eur. J. Med. Chem.* **2019**, *179*, 557–566, doi:10.1016/j.ejmech.2019.06.057.
16. Lenardão, E.J.; Santi, C.; Sancineto, L. *New Frontiers in Organoselenium Compounds*; Springer International Publishing: Cham, 2018; ISBN 978-3-319-92404-5.
17. Sies, H.; Parnham, M.J. Potential therapeutic use of ebselen for COVID-19 and other respiratory viral infections. *Free Radic. Biol. Med.* **2020**, *156*, 107–112, doi:10.1016/j.freeradbiomed.2020.06.032.
18. Sancineto, L.; Mariotti, A.; Bagnoli, L.; Marini, F.; Desantis, J.; Iraci, N.; Santi, C.; Pannecouque, C.; Tabarrini, O. Design and Synthesis of DiselenoBisBenzamides (DISEBAs) as Nucleocapsid Protein 7 (NCp7) Inhibitors with anti-HIV activity. *J. Med. Chem.* **2015**, *58*, 9601–9614, doi:10.1021/acs.jmedchem.5b01183.
19. Iraci, N.; Tabarrini, O.; Santi, C.; Sancineto, L. NCp7: targeting a multitask protein for next-generation anti-HIV drug development part 2. Noncovalent inhibitors and nucleic acid binders. *Drug Discov. Today* **2018**, *23*, 687–695, doi:10.1016/j.drudis.2018.01.022.
20. Sancineto, L.; Iraci, N.; Tabarrini, O.; Santi, C. NCp7: targeting a multitasking protein for next-generation anti-HIV drug development part 1: covalent inhibitors. *Drug Discov. Today* **2018**, *23*, 260–271, doi:10.1016/j.drudis.2017.10.017.
21. Krasowska, D.; Begini, F.; Santi, C.; Mangiavacchi, F.; Drabowicz, J.; Sancineto, L. Ultrasound-assisted synthesis of alkali metals diselenides (M₂Se₂) and their application for the gram-scale preparation of 2,2'-diselenobis(benzoic acid). *Arkivoc* **2019**, *2019*, 24–37, doi:10.24820/ark.5550190.p010.981.
22. Begini, F.; Krasowska, D.; Jasiak, A.; Drabowicz, J.; Santi, C.; Sancineto, L. Continuous flow synthesis of 2,2'-diselenobis(benzoic acid) and derivatives. *React. Chem. Eng.* **2020**, doi:10.1039/D0RE00012D.
23. Nascimento, V.; Cordeiro, P.S.; Arca, M.; Marini, F.; Sancineto, L.; Braga, A.L.; Lippolis, V.; Iwaoka, M.; Santi, C. Fast and easy conversion of ortho amidoaryldiselenides into the corresponding ebselen-like derivatives driven by theoretical investigations. *New J. Chem.* **2020**, *44*, 9444–9451, doi:10.1039/D0NJ01605E.
24. Pacuła, A.J.; Kaczor, K.B.; Antosiewicz, J.; Janecka, A.; Długosz, A.; Janecki, T.; Wojtczak,

- A.; Ścianowski, J. New Chiral Ebselen Analogues with Antioxidant and Cytotoxic Potential. *Molecules* **2017**, *22*, 492, doi:10.3390/molecules22030492.
25. Obieziurska, M.; Pacuła, A.J.; Długosz-Pokorska, A.; Krzemiński, M.; Janecka, A.; Ścianowski, J. Bioselectivity Induced by Chirality of New Terpenyl Organoselenium Compounds. *Materials (Basel)*. **2019**, *12*, 3579, doi:10.3390/ma12213579.
 26. O'Boyle, N.M.; Banck, M.; James, C.A.; Morley, C.; Vandermeersch, T.; Hutchison, G.R. Open Babel: An open chemical toolbox. *J. Cheminform.* **2011**, *3*, 33, doi:10.1186/1758-2946-3-33.
 27. Stewart, J.P. MOPAC2016 2016.
 28. Trott, O.; Olson, A.J. AutoDock Vina: Improving the speed and accuracy of docking with a new scoring function, efficient optimization, and multithreading. *J. Comput. Chem.* **2009**, NA-NA, doi:10.1002/jcc.21334.
 29. Seus, V.R.; Silva, L.; Gomes, J.; da Silva, P.E.A.; Werhli, A. V.; Machado, K.S. A framework for virtual screening. In Proceedings of the Proceedings of the 31st Annual ACM Symposium on Applied Computing - SAC '16; ACM Press: New York, New York, USA, 2016; pp. 31–36.
 30. Laskowski, R.A.; Swindells, M.B. LigPlot+: Multiple ligand-protein interaction diagrams for drug discovery. *J. Chem. Inf. Model.* **2011**, doi:10.1021/ci200227u.